Steeper Macular Curvature in Eyes With Non-Highly Myopic Retinitis Pigmentosa

Shiori Komori,[1] Shinji Ueno,[1] Yasuki Ito,[1] Akira Sayo,[1] Monika Meinert,[1,2] Taro Kominami,[1] Daiki Inooka,[1] Masahiro Kitagawa,[3] Kazuki Nishida,[4] Kunihiko Takahashi,[4] Shigeyuki Matsui,[4] and Hiroko Terasaki[1]

[1]Department of Ophthalmology, Nagoya University Graduate School of Medicine, Nagoya, Japan
[2]Department of Ophthalmology, Lund University, Lund, Sweden
[3]Nidek Co., Ltd., Gamagori, Japan
[4]Department of Biostatistics, Nagoya University Graduate School of Medicine, Nagoya, Japan

Correspondence: Shinji Ueno, Department of Ophthalmology, Nagoya University Graduate School of Medicine, 65 Tsuruma-cho, Showa-ku, Nagoya 466-8550, Japan; ueno@med.nagoya-u.ac.jp.

Submitted: April 14, 2019
Accepted: June 17, 2019

Citation: Komori S, Ueno S, Ito Y, et al. Steeper macular curvature in eyes with non-highly myopic retinitis pigmentosa. *Invest Ophthalmol Vis Sci*. 2019;60:3135–3141. https://doi.org/10.1167/iovs.19-27334

Purpose. A posterior staphyloma has been reported to be present in some eyes with retinitis pigmentosa (RP), and the purpose of this study was to determine the macular curvature of non-highly myopic RP eyes.

Methods. This was a retrospective, observational study. The medical charts of the right eyes of 143 patients with RP and 60 controls whose axial length ranged from 21.5 mm to 26.0 mm were reviewed. The mean curvature of Bruch's membrane within 6 mm of the central macula obtained from the horizontal optical coherence tomographic images were evaluated as the mean macular curvature index (MMCI). The relationships between the MMCI and other clinical factors were assessed.

Results. The mean MMCI of RP patients ($-13.73 \pm 9.63 \times 10^{-5}$ μm^{-1}) was significantly lower than that of the controls ($-6.63 \pm 5.63 \times 10^{-5}$ μm^{-1}). This indicated a deeper concave shape of the macula in RP eyes ($P < 0.001$). The MMCI was significantly correlated with the age ($r = 0.20$; $P = 0.016$) and the axial length ($r = -0.24$; $P = 0.004$). Further analysis suggested a nonlinear effect of the ellipsoid zone width on the macular curvature in the RP eyes.

Conclusions. There is a high incidence of steeper macular curvatures even in non-highly myopic RP eyes, and the steepness was also affected by the degree of photoreceptor degeneration.

Keywords: retinitis pigmentosa, optical coherence tomography, macular curvature

A posterior staphyloma is defined as an outpouching of the sclera with its radius of curvature shorter than the radius of curvature of the surrounding eye wall.[1] A staphyloma is observed in optical coherence tomographic (OCT) images as an excavation of the posterior pole. This unusual morphologic shape is usually found in highly myopic eyes, and it is very rare in non-highly myopic eyes.[2]

A posterior staphyloma has also been reported to be present in eyes with various inherited retinal degenerative diseases even in non-highly myopic eyes. These diseases include eyes with microcornea, rod-cone dystrophy, cataract, posterior staphyloma syndrome,[3] Leber's congenital amaurosis that is caused by variants of *RDH12* gene,[4] Joubert syndrome,[5] retinal ciliopathy with *C21orf2* variants,[6] and retinitis pigmentosa (RP).[7,8] These case reports suggested that a retinal degeneration can not only change the morphology of the neurosensory retina but also alter the eye shape including the macula. However, the incidence and characteristics of eyes affected by a posterior staphyloma in eyes with inherited retinal diseases have not been determined.

The ability of OCT to record cross-sectional images of the posterior pole has enabled clinicians to examine the overall eye shape. Quantitative morphologic investigations of the posterior pole have been performed in eyes with high myopia using OCT images.[9] In addition, similar types of analyses have been performed in a community-based cohort.[2] Although the staphylomas in highly myopic eyes have been examined in detail, similar analyses have not performed on eyes with RP.

Thus, the purpose of this study was to determine the macular shape of 143 eyes with RP and to assess the characteristics of the eye that affect the macular shape.

Methods

All of the procedures used in this retrospective study adhered to the tenets of the Declaration of Helsinki, and the Institutional Review Board/Ethics Committee of the Nagoya University Hospital approved this study (no. 2016-0538-2). The Institutional Review Board also waived the need for a written informed consent from each patient because the study design was a retrospective chart review.

Subjects

We reviewed the medical records of 303 RP patients who were examined by one of the authors (SU) at the Nagoya University Hospital between March 2013 and December 2017. The

diagnosis of RP was based on the presence of night blindness, constriction of the visual fields, attenuation of retinal vessels, bone-spicule pigmentation, and reduced (<100 μV) or extinguished full-field scotopic flash electroretinograms elicited by 300 cd-s/m^2 (electroretinography; PE300; TOMEY, Nagoya, Japan). The data of only the right eyes of the 303 patients were used for the statistical analyses. Of the 303 potential patients, 162 patients had spectral-domain OCT (SD-OCT; Heidelberg Engineering, Heidelberg, Germany) images recorded. The images were of 9-mm radial scans. The axial length (AL) of these eyes ranged from 21.5 mm and 26.0 mm (IOL Master; Carl Zeiss Meditec, Inc., Dublin, CA, USA). Eyes with poor-quality OCT images due to severe cataract or inadequate location of the fovea due to poor fixation were excluded. In the end, 143 right eyes of 143 RP patients were analyzed. The most recent data were used for statistical analyses. The data of 60 normal right eyes were collected in the same way, and their data were compared with that of the RP patients.

The best-corrected visual acuity (BCVA) that was determined on the same day as the recording of the OCT images was used for the statistical analyses. The decimal BCVA was converted to logarithm of the minimum angle of resolution (logMAR) units for the statistical analyses. Counting fingers, hand motion, light perception, and no light perception were designated as 1.85, 2.30, 2.80, and 2.90 logMAR units respectively.[10]

Measurement of Retinal Morphologic Parameters in SD-OCT Images

We examined the horizontal scan images that were composed of 100 averaged images with the eye tracking system functioning. The size of each OCT image was adjusted to correct for the difference in the pixel resolution in the transverse and longitudinal directions.

The ellipsoid zone (EZ) width was measured between the borders where the EZ band met the upper surface of the retinal pigment epithelium (RPE) by using the built-in caliper.[11] If the EZ width exceeded the scanned images, the border of the EZ was set as the edge of the scanned image. All of the measurements were performed using the Heidelberg Eye Explorer software (Heidelberg Engineering).

Measurements of Macular Curvature

The reflective line corresponding to Bruch's membrane across the fovea was analyzed quantitatively using the Matlab software (The MathWorks, Inc., Natick, MA, USA). Twelve points on the Bruch's membrane line were marked beginning from the fovea, and the marks were separated by 76 μm in the SD-OCT images (Fig. 1A). The software calculated the approximate curvature of the marked points using cubic spline interpolation (yellow and red line in Fig. 1B). The cubic spline (S) consists of 11 sections of cubic polynomials, and every 2 adjacent sections, S_i and S_{i+1}, satisfied the following conditions on each marked point, p_i, so that the sections were smoothly connected to the surrounding points:

- $S_0(x_0) = y_0$
- $S_i(x_{i+1}) = y_{i+1} = S_{i+1}(x_{i+1})$
- $S'_i(x_{i+1}) = S'_{i+1}(x_{i+1})$
- $S''_i(x_{i+1}) = S''_{i+1}(x_{i+1})$

where x_i and y_i are the horizontal and vertical coordinates of the marked point p_i, respectively. Note that each section, S_i, connects points p_i and p_{i+1}; thus, its domain of definition is $x_i \leq x \leq x_{i+1}$.

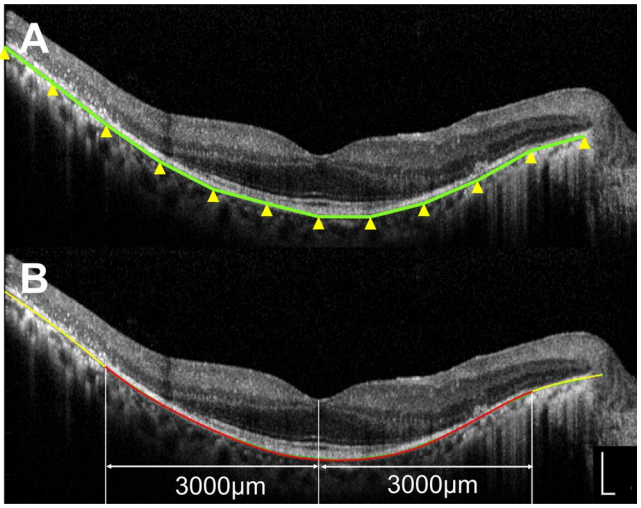

FIGURE 1. Method used to quantify the macular curvature from an SD-OCT image. (**A**). SD-OCT image of 9-mm scan. Twelve points (*yellow arrowheads*) are plotted on Bruch's membrane within 200 pixels from the center of the fovea, with 5 points on the nasal side and 6 points on the temporal side. (**B**). The software calculates the approximate curvature (*yellow* and *red line*) from the marked 12 points in (**A**). From the calculated curve, the curvatures for 3 mm from the central fovea in the temporal and nasal side are selected (*red line*). The software calculates the mean of the curvature from all measured values in this selected range in 1-μm steps. *Scale bars*: 200 μm.

From the calculated curves, we chose the curvature in the range of 6 mm including the central fovea (red line in Fig. 1B), and the curvature values outside of this range (yellow line in Fig. 1B) were not used to reduce the effects of the optic disc.

The curvature value $\kappa(x)$ is calculated as

$$\kappa(x) = S''(x)/\left(1+(S'(x))^2\right)^{\frac{3}{2}}$$

and the differentials, S' and S", were obtained from the coefficients of the cubic spline. The software calculated the mean curvature between ±3 mm from the central fovea by using all measured values for the local curvature in 1-μm steps. We named this value the mean macular curvature index (MMCI), and its unit was μm^{-1}.

Statistical Analyses

Mann-Whitney *U* tests and Fisher's exact tests were used to determine the significance of the differences in the continuous and categorical variables, respectively. The intraclass correlation coefficient was determined with a two-way mixed-effect model to assess the reliability of the curvature measurements by the graders. The correlations between the MMCIs and various ocular parameters were analyzed using rank correlation coefficients. Multiple linear regression analysis was performed to evaluate the associations between the MMCIs and other factors, including the category of RP or control, sex, AL, and age. For the secondary analyses, we conducted local regression (locally estimated scatterplot smoothing [LOESS]), which is a procedure for fitting a regression surface to data through multivariate smoothing, to consider the nonlinear relationships of the EZ width and MMCIs in RP eyes.[12] To confirm the nonlinear effect of the EZ width on the MMCIs, we divided the EZ width into three groups, namely, short, intermediate, and long, by using the k-means clustering method, and we performed one-factor ANOVA and Mann-Whitney *U* tests between each three groups. A *P* value of <0.05 was considered to be statistically significant. All statistical analyses were

Table 1. Clinical Characteristics of RP Patients and Control Groups

	RP ($n = 143$)		Control ($n = 60$)		
Parameter	Mean ± SD	Median (IQR)	Mean ± SD	Median (IQR)	*P* Value
Age, y	48.62 ± 16.26	48.00 (35.50 to 60.00)	47.30 ± 17.79	47.50 (31.00 to 63.00)	0.57
AL, mm	23.83 ± 1.02	23.75 (23.12 to 24.53)	24.08 ± 0.93	24.05 (23.48 to 24.82)	0.074
BCVA, logMAR	0.43 ± 0.65	0.22 (0.00 to 0.52)	NA	NA	NA
MMCI, $\times 10^{-5}$, μm^{-1}	−13.73 ± 9.63	−11.93 (−19.75 to −7.31)	−6.63 ± 5.63	−6.44 (−10.90 to −2.38)	<0.001*
EZ width, μm	2227.29 ± 2269.09	1714.00 (0.00 to 3751.00)	NA	NA	NA

IQR, interquartile range; NA, not available.
* Statistical significance by Mann-Whitney *U* test ($P < 0.001$).

performed with R software version 3.4.3 and EZR software version 1.36 (Saitama Medical Center, Jichi Medical University, Saitama, Japan).[13]

Results

Clinical Characteristics of RP and Control Eyes

The demographic and clinical characteristics of the eyes of 60 men and 83 women with RP and the eyes of 24 men and 36 women as controls are shown in Table 1. There were no differences in the sex distribution, age, and AL between the RP and control eyes. The median of the BCVA was 0.22 logMAR units for the RP group. The EZ was intact in all of the control eyes but partially or fully disrupted in all of the RP eyes.

The intraclass correlation coefficient for the MMCI between the two graders (SK and MM) for the 104 eyes was 0.98. The data obtained by SK were used for the statistical analyses.

The MMCI in the control eyes was $-6.63 \pm 5.63 \times 10^{-5}$ μm^{-1} and that for the RP eyes was $-13.73 \pm 9.63 \times 10^{-5}$ μm^{-1}, which indicated that the curvature of the control was less concave than that of the RP eyes (Table 1). The minus values indicate a concave shape and plus values indicate a convex shape. The results suggested that the macular shape was a steeper concave in the RP eyes.

Representative OCT Images of Control and RP Patients

The horizontal scanned SD-OCT images and fundus photographs of one control eye and four eyes with different degrees of severity of RP (cases 1–4) are shown in Figure 2. The control patient was a 22-year-old woman (Fig. 2A). Her macular shape was flat, and this was confirmed by our calculation that the MMCI was -0.69×10^{-5} μm^{-1}. Her AL was 24.66 mm.

Case 1 was a 43-year-old woman with early stage RP that was a representative case with a preserved long EZ of 6131 μm (Fig. 2B). Bruch's membrane was more curved around the area of the disruptive EZ. The MMCI was -17.1×10^{-5} μm^{-1}, and the AL was 24.74 mm. Case 2 was a 46-year-old man who is a representative case with relatively advanced RP with an EZ of 3020 μm (Fig. 2C). Bruch's membrane of case 2 had a steeper curvature than that of case 1. The MMCI was -22.5×10^{-5} μm^{-1}, and the AL was 22.91 mm. Case 3 was a 37-year-old man who is a representative case with advanced RP with a completely disrupted EZ (0 μm) (Fig. 2D). The OCT image showed a posterior staphyloma, and the MMCI was -34.5×10^{-5} μm^{-1}. The AL was 24.53 mm. Case 4 was a 70-year-old woman who is also a representative case with advanced RP without an intact EZ (0 μm) (Fig. 2E). However, this patient had a relatively flat macular line, the MMCI was -6.76×10^{-5} μm^{-1}, and the AL was 23.38 mm.

Distribution of MMCIs of Control and RP Eyes

The distributions of the MMCIs of the controls and RP eyes are shown in Figure 3. For the controls, the MMCI ranged from -20×10^{-5} μm^{-1} to 10×10^{-5} μm^{-1} except for 1 eye. The MMCI of 24% (35/143) of the RP patients was lower than -20×10^{-5} μm^{-1}, and the range of the MMCIs was greater than that of the control eyes. In addition, the ratio of the flat to upward convex, i.e., plus MMCI, in the RP eyes was significantly smaller than that of control eyes ($P < 0.05$). The percentage of eyes with the steep curvature less than -25×10^{-5} μm^{-1} that was detected as a distinct excavation of the posterior pole was 12% of the RP eyes (17/143). In this group, all patients were younger than 70 years, and none had an EZ length >5400 μm. There were no differences in the sex distribution ($P = 0.79$), age, AL, BCVA, and EZ width between them and other RP eyes ($P = 0.15$, $P = 0.45$, $P = 0.88$, and $P = 0.85$; respectively).

Correlations Between MMCI and Clinical Parameters

To determine which factors including RP or control, AL, sex, and age were significantly associated with the MMCI, we performed multiple linear regression analyses. The results showed that the category, RP or control, and the AL were significant independent factors for predicting the MMCI (Table 2). The coefficient for the category, RP or control, was −7.75 and that for the AL was −2.11, which suggested that the category of RP and longer AL were significantly correlated with lower MMCI values.

Next, we determined the correlations between the MMCI and the age, AL, BCVA, and EZ width of the RP eyes (Table 3). The MMCI was significantly correlated with the age and the AL, although the correlation coefficients were low (Table 3; Supplementary Fig. S1). The MMCI was not correlated with the BCVA and the EZ width.

Nonlinear Effect of EZ Width on Macular Curvature in RP Eyes

Our results showed that the macular curvature was concave and steeper in patients with shorter EZ (see cases 1 and 2). However, some patients with blurred or no measurable EZ had steep macular curvature as shown in case 3 and others had flat to convex as in case 4. We suggest that the variability of the MMCI in advanced RP might be the reason why the linear correlation of the EZ width with the MMCI was not significant.

The LOESS curve and scatterplots of the EZ width and MMCIs in RP eyes suggested a nonlinear effect of the EZ width on the MMCI. The MMCI was lowest in eyes with an EZ width of around 2200 μm, and the MMCI was higher in the eyes with shorter or longer EZ widths (Fig. 4A). Thus, we performed additional analyses by dividing the RP patients into three groups according to the width of the EZ using k-means

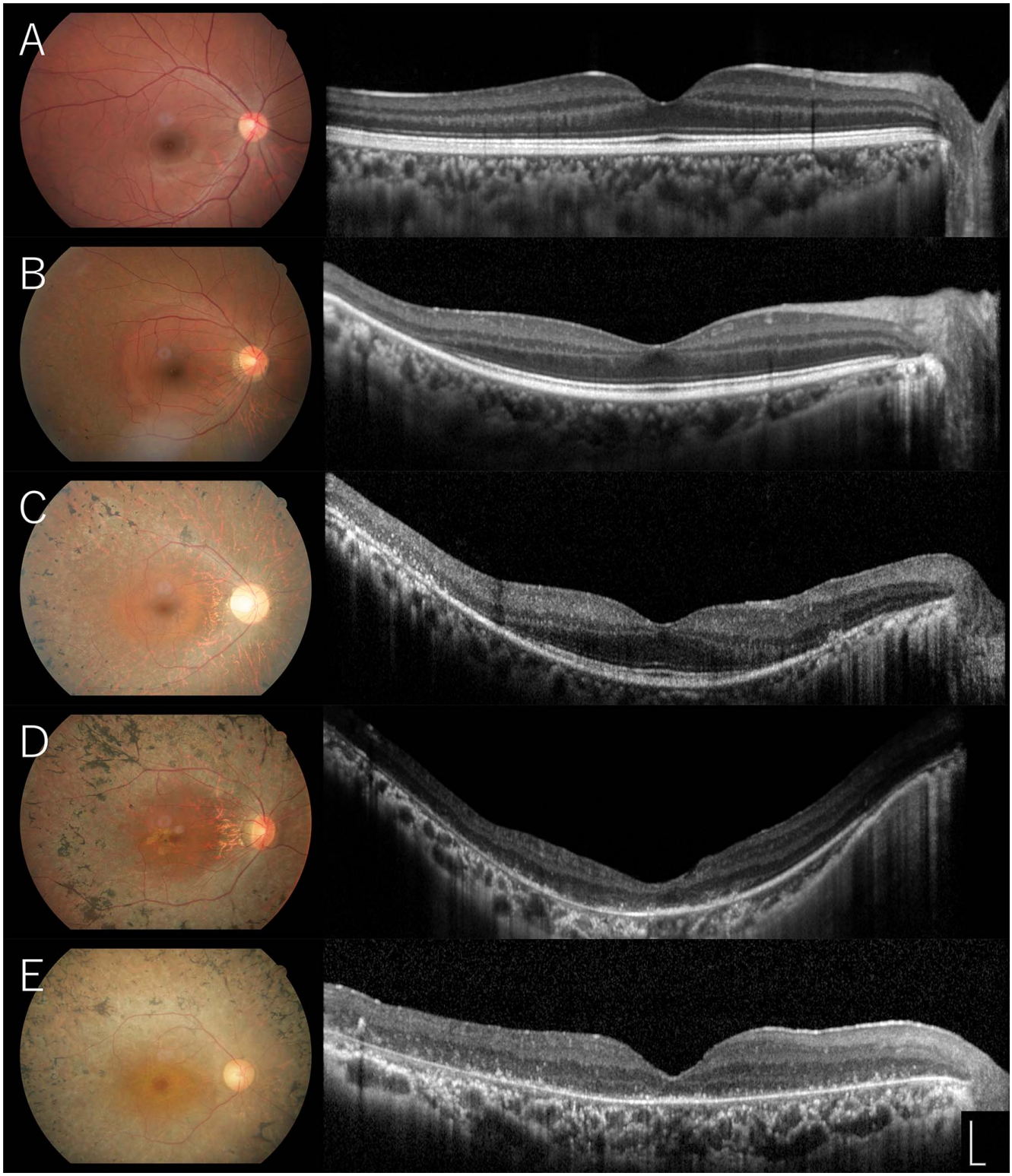

Figure 2. Representative OCT images of control and RP patients. (**A**) Fundus photograph and SD-OCT images of a control case whose AL was 24.66 mm. The shape of the macula is flat, and the MMCI was -0.69×10^{-5} μm^{-1}. (**B**) Representative eye with a long EZ width (case 1). The MMCI was -17.1×10^{-5} μm^{-1}, and the AL was 24.74 mm. (**C**) Representative eye with relatively advanced RP with intermediate EZ width (case 2). OCT shows a steeper curvature of Bruch's membrane than that of case 1. The MMCI was -22.5×10^{-5} μm^{-1} and the AL was 22.91 mm. (**D**) Representative eye with advanced RP with blurred EZ (case 3). The OCT shows a posterior staphyloma, and the MMCI was -34.5×10^{-5} μm^{-1}. The AL was 24.53 mm. (**E**) A representative case with advanced RP without an intact EZ (case 4). The eye had a relatively flat macular outline, and the MMCI was -6.76×10^{-5} μm^{-1}. The AL was 23.38 mm. *Scale bar*: 200 µm.

Investigative Ophthalmology & Visual Science

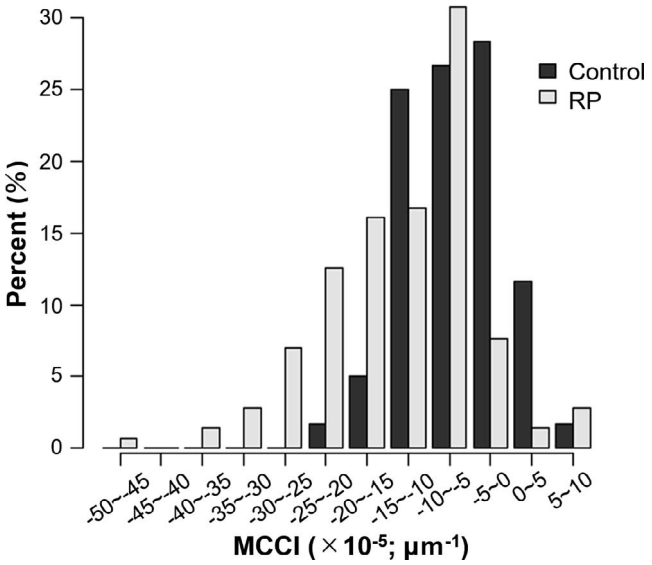

FIGURE 3. Incidence of MMCI of eyes of controls and RP patients. The distribution of the MMCIs in the control (*black bar*) and RP (*gray bar*) eyes.

clustering. The eyes with EZ width ranging from 0 to 1311 μm were designated as having short EZs, ($n = 61$), from 1312 to 3842 μm were designated as having intermediate EZs, ($n = 48$), and ≥3843 μm were designated as having long EZs ($n = 34$). The differences of the MMCI in the three groups were significant ($P < 0.05$). The mean MMCI in the intermediate group was significantly lower than that of the short and long groups ($P < 0.05$) (Fig. 4B).

DISCUSSION

Our results showed that the macular curvature of the 143 non-highly myopic RP eyes had a significantly steeper concave curvature of the macula than that of the control group. Further analysis showed a nonlinear effect of the EZ width on the macular curvature in the RP eyes. These findings suggested that the normal layers of the retina and RPE need to be intact to support the flatness of the macular shape. The unit of MMCI might be ambiguous and not relevant in the analysis of the curvature, and the radius of the curvature might be better. However, the value of the radius of curvature became close to infinity in cases of a flat macula, which made statistical analyses not possible. Thus, we used MMCI, which is the inverse of the radius of curvature.

Recently, Xu et al.[8] studied 13 eyes of 7 RP patients with a macular staphyloma in non-highly myopic eyes. They reported that the type of staphyloma in these RP patients was different from that in pathologic myopia, and the staphylomas found in RP eyes belonged to the narrow macular staphyloma type, whereas the wide macular staphyloma type, equivalent of type I in classification by Curtin,[14] was the predominant type of staphylomas in highly myopic eyes.[15] In our RP group, we found 17 eyes with a highly curved shape (MMCI, less than -25×10^{-5} μm^{-1}), which might be classified as eyes with a staphyloma. As shown in case 3, most of these eyes were also classified as the narrow macular staphyloma type. However, the definition of staphyloma in OCT scan images, which analyzes a limited area of posterior pole, has not been established. Thus, we evaluated the macular shape quantitatively by modifying the way of analysis used in a previous study of highly myopic eyes.[9] Our quantitative analysis allowed us to analyze the distribution of the macular curvature in RP patients and also to identify the RP eyes with abnormally steep curvature. This method for evaluating the fundus shape will allow clinicians to investigate eyes with not only high myopia but also retinal degeneration.

TABLE 2. Multiple Linear Regression Analysis of Independent Factors Associated With the MMCI

Variable Independent	β (95% CI)	*P* Value
Group (ref = Control)	−7.75 (−10.30 to −5.19)	<0.001†
AL, mm	−2.11 (−3.36 to −0.86)	0.001*
Sex (ref = Male)	1.38 (−1.09 to 3.85)	0.27
Age, y	0.06 (−0.01 to 0.13)	0.098

Multiple linear analysis; adjusted *R*-squared = 0.18; β = standard partial regression coefficient. ref, reference.
* Statistical significance ($P < 0.05$).
† Statistical significance ($P < 0.001$).

Our data showed that not only the status of the RP but also the AL was an independent predictor of the degree of curvature, which is consistent with an earlier study on a large population-based cohort.[2] The AL would affect the macular curvature in the normal and RP eyes.

We hypothesized that the photoreceptor degeneration was associated with the formation of a posterior staphyloma, but the EZ width was not correlated linearly with the MMCI. Thus, we examined the relationship between the EZ width and MMCI by additional analyses. As expected, a shortening of the EZ made the macular curvature steeper in the eyes with EZ of greater than 2200 μm (Fig. 4A). However, a further shortening of the EZ made the macular curvature flatter in the eyes with EZ of less than 2200 μm. In addition, the eyes with intermediate EZ had significantly lower MMCI than eyes with short EZ, i.e., EZ of <1311 μm. There are several possible reasons for the higher MMCI in the eyes with short EZ. One is the flattening of the macular curvature by the further reduction of the central EZ in the end stage of RP. The macular shape is bowing in accordance with the reduction of EZ in the relatively peripheral area, but during or after the disturbances of the EZ in the central macular it might be stretched. To prove this possibility, longitudinal observational studies will be needed. The second explanation is the great heterogeneity of macular involvement among RP patients illustrated by the large number of causative genes, which cause various underlying biochemical pathways.[16–18] In certain RP subtypes, macular degeneration occurs relatively early in the disease course.[19] In this type, the EZ in the macular area might disappear evenly, which is different from a shorting of the EZ, and the curvature might be unchanged. This type of RP eyes would be classified as the short EZ group, and they may have the short EZ and cause the high variations in the curvature in zero EZ width patients.

The formation of a posterior staphyloma has been reported to be associated with the mutation of several genes especially in the phenotype of early-onset retinal dystrophy: *RDH*12,[4] *C21orf2*,[6] *DHX38*,[20] *IDH3A*,[21] and *NMNAT1*.[22] We included

TABLE 3. Correlation With the MMCI and Clinical Parameters in RP

Parameters	r	*P* Value
Age, y	0.20	0.016*
AL, mm	−0.24	0.004*
BCVA, logMAR	0.11	0.18
EZ width, μm	−0.001	0.99

Pearson tests; r = correlation coefficient.
* Statistical significance ($P < 0.05$).

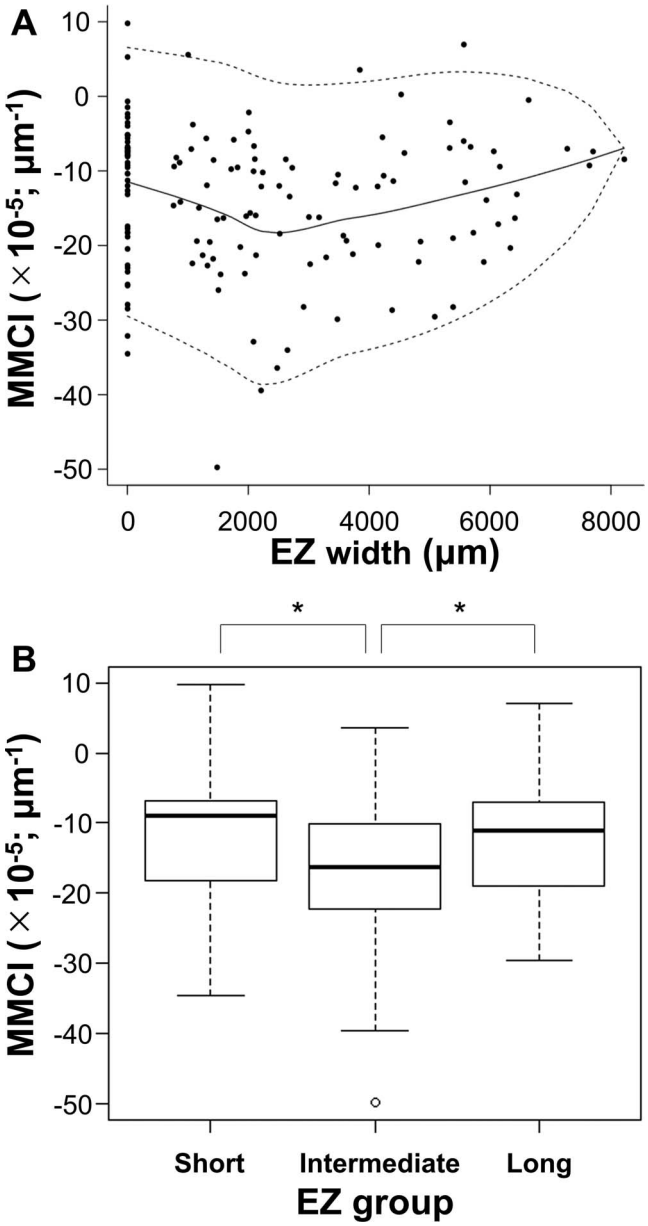

Figure 4. Relation of MMCI and EZ width. (**A**) The locally estimated scatterplot smoothing (LOESS) curve and scatterplots for the EZ width and the MMCIs in RP eyes. The solid curve displays the fitted value. The pair of dotted curves is the estimated 95% prediction intervals. Scatter plots illustrating correlation between the MMCI and EZ width. (**B**) Box plots showing the distribution of the MMCIs according to the EZ width. Eyes with RP are divided into 3 groups, namely, short EZ (0 to 1311 µm; $n = 61$), intermediate EZ (1312 µm to 3842 µm; $n = 48$), and long EZ (3843 µm or greater; $n = 34$). The MMCI in the intermediate group was significantly lower than that of the short and long EZ groups. *Asterisks* show statistical significance (Mann-Whitney U test; $^*P < 0.05$).

only the patients older than 10 years. When we investigated the eyes with relatively younger patients, the mean ± SD MMCI of six eyes in the teens was $-7.45 \pm 8.27 \times 10^{-5}$ µm^{-1} and only one patient was less than -20×10^{-5} µm^{-1} (Supplementary Fig. S1). This indicates that the cases with early-onset of RP did not always have steep curvatures of the posterior pole. However, the quantitative analysis of the macular curvature in earlier onset RP cases, including Leber congenital amaurosis, might be different. In adult RP cases, several eyes with posterior staphyloma were reported,[7,8] but in most of the cases the causative genes were unidentified except one patient with the *EYS* pathogenic variant.[8] We did not analyze the genotype-phenotype correlations because of the lack of the number of patients who were identified by causative gene variants. To detect the mechanism of steep curvature in RP, further evaluations of the associated genes and macular curvatures need to be performed.

There are several limitations in our study. First, we analyzed only the horizontal scans of the OCT images. It might be better to analyze the macular shape in three dimensions by the volume scans of the macular area or in both the vertical and horizontal images. Our software did not allow us to analyze the volume scans and lack of vertical OCT images in some patients permitted us to analyze the horizontal scan images. Although the horizontal curvature seems to be representative for the macular curvature, our results might have limited aspects of the macular shape in RP eyes. Second, evaluations of 6-mm width from the 9-mm OCT scan width might not be wide enough to determine the relationship of the retinal degeneration and the curvature. The retinal degeneration proceeds from the peripheral retina to the macular area, and the evaluation of curvature in more peripheral area would be worth performing. To examine the curvature in the peripheral retina, a wide scan range by swept source OCT might be better. Third, this study did not find a significant relationship between the MMCI and macula function. The effect of the curvature on the macula function, which can be estimated by focal and multifocal ERGs, will be determined in a future study. Fourth, due to the cross-sectional study design, it remains unclear whether the curvature changes were associated with the development of retinal degeneration.

In conclusion, our results show a high incidence of steep macular curvature in RP eyes. Although we did not find the factors that play a crucial role in the formation of the curvature, the steepness of macular curvature in RP was affected by the EZ width. To date, the importance of macular curvature has not been determined in RP eyes, but it is reported that patients with abnormal posterior concavity of the eye wall should not be considered ideal candidates for implantation of retinal prosthesis because the signal transduction from electrodes to retinal target cells appears to be counteracted by an excessive electrode-retina distance.[7] Further quantitative analysis in larger cohorts of RP with genetic analysis would make it possible to determine the mechanisms and importance of the curvature in eyes with RP.

Acknowledgments

The authors thank Duco Hamasaki, PhD (Bascom Palmer Eye Institute) for the discussions and editing the final version of the manuscript.

Supported in part by the Japan Society for the Promotion of Science (JSPS) KAKENHI Grant Numbers 16K11320 to S.U., 16K11265 to Y.I., and Takayanagi Retina Research Award to S.U.

Disclosure: **S. Komori**, None; **S. Ueno**, None; **Y. Ito**, None; **A. Sayo**, None; **M. Meinert**, None; **T. Kominami**, None; **D. Inooka**, None; **M. Kitagawa**, None; **K. Nishida**, None; **K. Takahashi**, None; **S. Matsui**, None; **H. Terasaki**, None

References

1. Ohno-Matui K. Staphyloma. In: Spaide RF, Ohno-Matsui K, Yannuzzi LA, eds. *Pathologic Myopia*. New York, NY: Springer; 2014:167–176.
2. Numa S, Yamashiro K, Wakazono T, et al. Prevalence of posterior staphyloma and factors associated with its shape in the Japanese population. *Sci Rep*. 2018;8:4594.

3. Reddy MA, Francis PJ, Berry V, et al. A clinical and molecular genetic study of a rare dominantly inherited syndrome (MRCS) comprising of microcornea, rod-cone dystrophy, cataract, and posterior staphyloma. *Br J Ophthalmol*. 2003; 87:197–202.
4. Kuniyoshi K, Sakuramoto H, Yoshitake K, et al. Longitudinal clinical course of three Japanese patients with Leber congenital amaurosis/early-onset retinal dystrophy with *RDH*12 mutation. *Doc Ophthalmol*. 2014;128:219–228.
5. Toma C, Ruberto G, Marzi F, et al. Macular staphyloma in patients affected by Joubert syndrome with retinal dystrophy: a new finding detected by SD-OCT. *Doc Ophthalmol*. 2018; 137:25–36.
6. Khan AO, Eisenberger T, Nagel-Wolfrum K, et al. *C21orf2* is mutated in recessive early-onset retinal dystrophy with macular staphyloma and encodes a protein that localises to the photoreceptor primary cilium. *Br J Ophthalmol*. 2015;99: 1725–1731.
7. Parmeggiani F, De Nadai K, Piovan A, et al. Optical coherence tomography imaging in the management of the Argus II retinal prosthesis system. *Eur J Ophthalmol*. 2017;27:e16–e21.
8. Xu X, Fang Y, Yokoi T, et al. Posterior staphylomas in eyes with retinitis pigmentosa without high myopia. *Retina*. 2018; 38:2277–2434.
9. Miyake M, Yamashiro K, Akagi-Kurashige Y, et al. Analysis of fundus shape in highly myopic eyes by using curvature maps constructed from optical coherence tomography. *PLoS One*. 2014;9:e107923.
10. Schulze-Bonsel K, Feltgen N, Burau H, et al. Visual acuities "hand motion" and "counting fingers" can be quantified with the freiburg visual acuity test. *Invest Ophthalmol Vis Sci*. 2006;47:1236–1240.
11. Kominami T, Ueno S, Kominami A, et al. Associations between outer retinal structures and focal macular electroretinograms in patients with retinitis pigmentosa. *Invest Ophthalmol Vis Sci*. 2017;58:5122–5128.
12. William S, Susan J. Locally weighted regression: an approach to regression analysis by local fitting. *J Am Stat Assoc*. 1988; 83:596–610.
13. Kanda Y. Investigation of the freely available easy-to-use software 'EZR' for medical statistics. *Bone Marrow Transplant*. 2013;48:452–458.
14. Curtin BJ. The posterior staphyloma of pathologic myopia. *Trans Am Ophthalmol Soc*. 1977;75:67–86.
15. Ohno-Matsui K. Proposed classification of posterior staphylomas based on analyses of eye shape by three-dimensional magnetic resonance imaging and wide-field fundus imaging. *Ophthalmology*. 2014;121:1798–1809.
16. Cai CX, Locke KG, Ramachandran R, et al. A comparison of progressive loss of the ellipsoid zone (ez) band in autosomal dominant and X-linked retinitis pigmentosa. *Invest Ophthalmol Vis Sci*. 2014;55:7417–7422.
17. Sujirakul T, Lin MK, Duong J, et al. Multimodal imaging of central retinal disease progression in a 2-year mean follow-up of retinitis pigmentosa. *Am J Ophthalmol*. 2015;160:786–798.
18. Sayo A, Ueno S, Kominami T, et al. Longitudinal study of visual field changes determined by Humphrey Field Analyzer 10-2 in patients with Retinitis Pigmentosa. *Sci Rep*. 2017;7:16383.
19. Flynn MF, Fishman GA, Anderson RJ, Roberts DK. Retrospective longitudinal study of visual acuity change in patients with retinitis pigmentosa. *Retina*. 2001;21:639–646.
20. Ajmal M, Khan MI, Neveling K, et al. A missense mutation in the splicing factor gene *DHX38* is associated with early-onset retinitis pigmentosa with macular coloboma. *J Med Genet*. 2014;51:444–448.
21. Pierrache LHM, Kimchi A, Ratnapriya R, et al. Whole-exome sequencing identifies biallelic *IDH3A* variants as a cause of retinitis pigmentosa accompanied by pseudocoloboma. *Ophthalmology*. 2017;124:992–1003.
22. Koenekoop RK, Wang H, Majewski J, et al. Mutations in *NMNAT1* cause Leber congenital amaurosis and identify a new disease pathway for retinal degeneration. *Nat Genet*. 2012;44: 1035–1039.

Investigative Ophthalmology & Visual Science